Magnetic and hyperfine properties of nanocrystalline $Ni_{0.2}Zn_{0.6}Cu_{0.2}Fe_2O_4$ prepared by a chemical route

2006 J. Phys.: Condens. Matter 18 5253

(http://iopscience.iop.org/0953-8984/18/22/023)

INSTITUTE OF PHYSICS PUBLISHING JOURNAL OF PHYSICS: CONDENSED MATTER

J. Phys.: Condens. Matter **18** (2006) 5253–5267 doi:10.1088/0953-8984/18/22/023

Magnetic and hyperfine properties of nanocrystalline $Ni_{0.2}Zn_{0.6}Cu_{0.2}Fe_2O_4$ prepared by a chemical route

P K Chakrabarti[1,7], B K Nath[2,3], S Brahma[1], S Das[4], K Goswami[4], U Kumar[5], P K Mukhopadhyay[5], D Das[3], M Ammar[6] and F Mazaleyrat[6]

[1] Department of Physics, Asutosh College, 92, S.P. Mukherjee Road, Kolkata 700 026, India
[2] Department of Physics, Sundarban Mahavidyalaya, South 24 Pgs, West Bengal 743 347, India
[3] UGC-DAE CSR (formerly IUC-DAEF CC), III/LB-8, Bidhannagar, Kolkata 700 098, India
[4] Department of Physics, Jadavpur University, Kolkata 700 032, India
[5] S N Bose National Centre for Basic Sciences, Bidhannagar, Kolkata 700 098, India
[6] Ecole Normale Supérieure de Cachan, SATIE CNRS UMR8029, 61 Avenue du Président Wilson, 94235 Cachan, France

E-mail: pabitra_c@hotmail.com (P K Chakrabarti)

Received 15 February 2006, in final form 5 April 2006
Published 19 May 2006
Online at stacks.iop.org/JPhysCM/18/5253

Abstract

Nanoparticles of $Ni_{0.2}Zn_{0.6}Cu_{0.2}Fe_2O_4$ were prepared by the standard co-precipitation method. The formation of nanocrystalline mixed spinel phase has been confirmed by x-ray diffractograms. The sizes of the nanoparticles were estimated in the range 7–30 nm, which was confirmed by transmission electron microscopy. Thermal variations of the real part of AC magnetic susceptibilities measured from 450 K down to 80 K and Mössbauer effect measurements at room temperature and down to 20 K clearly indicate the presence of superparamagnetic particles in all the samples. Specific saturation magnetizations measured by VSM are found to increase steadily with the increase of average particle size. The coercive field obtained from low frequency measurements shows that in all the samples a small fraction of particles is not relaxed within the measuring time. For samples showing a less dominating superparamagnetic behaviour, AC magnetic susceptibility data showed the expected increase of blocking temperature with increase in particle size. Magnetic anisotropy energy constants of the nanoparticles were estimated from the blocking temperature and the values cannot be directly correlated with their particle sizes.

[7] Author to whom any correspondence should be addressed.

1. Introduction

Magnetic nanoparticles of mixed spinel ferrites have been the subject of current interest because of their interesting magnetic, electric, dielectric and optical properties, which are considerably different from that of their bulk counterparts [1–4]. These systems are commercially important for their several applications in electromagnetic devices operating in the radio frequency region where the superparamagnetic (SPM) properties have a strong influence on enhancing their quality of applications [5–7]. Nanoparticles of these materials exhibit interesting phase transitions from superparamagnetic to ferri/ferro-magnetic state or vice versa with variation of temperatures depending on their sizes. Major factors that control superparamagnetism are magnetic anisotropy and volume of nanoparticles. The factors that govern the value of magnetic anisotropy are electron spin–orbital angular momentum coupling at lattice sites, dipole–dipole interaction among the magnetic ions, shape of nanoparticles etc. The strength of the spin–orbital angular momentum coupling depends mainly on the value of magnetic moment of the atoms involved in the coupling, their relative distances and the symmetry of the lattice site. To achieve SPM properties with relatively large sizes of nanoparticles these factors can be systematically varied, particularly in the case of mixed spinel ferrites [8–11].

Among the mixed spinel ferrite, nickel–zinc ferrite is an important soft magnetic material because of low coercive field, high resistivity and low production cost. Its resistivity is $\sim 10^8$ Ω m, which is very high compared to Mn–Zn ferrite (1 Ω m only). In this ferrite, nonmagnetic Zn^{2+} ions occupy tetrahedral A-sites replacing Fe^{3+} ions, which eventually go to octahedral B-sites. Hence zinc cations magnetically dilute the system by making the A–B exchange interaction relatively weaker. This weaker coupling reduces the anisotropy energy of the system, which facilitates the onset of SPM relaxation in bigger size particles even at room temperature. Recently, multi-layer chip inductors (MLCIs) have drawn much attention for their applications in communicative electronic devices [12, 13]. Mixed spinel Ni–Zn ferrite prepared at low annealing temperature has been used as magnetic material for MLCIs for its good electromagnetic properties. The substitution of Cu^{2+} in Ni–Zn ferrite enhances the possibility of its application as an MLCI in the high frequency regime [6, 7, 14, 15] because it lowers the sintering temperature to about 900 °C.

In the present paper, we report the preparation of mixed spinel $Ni_{0.2}Zn_{0.6}Cu_{0.2}Fe_2O_4$ ferrite of different grain sizes by the standard co-precipitation method and its structural and magnetic characterization by XRD, Mössbauer spectroscopy, VSM and AC magnetic susceptibility. In order to get different sizes of the nanoparticles, the as prepared sample was heat-treated at different temperatures from 200 to 900 °C.

2. Experimental details

Mixed spinel $Ni_{0.2}Zn_{0.6}Cu_{0.2}Fe_2O_4$ ferrite was prepared by the standard co-precipitation method. Anhydrous ferric chloride ($FeCl_3$), nickel chloride ($NiCl_2{\cdot}6H_2O$), anhydrous zinc chloride ($ZnCl_2$) and copper nitrate ($Cu(NO_3)_2{\cdot}3H_2O$) were used as starting materials and a completely homogeneous solution of these salts was prepared by dissolving the salts in deionized water. A few drops of concentrated hydrochloric acid were added to obtain a clear solution. The stoichiometric ratio of Fe:Ni:Zn:Cu was taken as 2:0.2:0.6:0.2. The solution was then heated to about 80 °C. NaOH solution (0.4 M l^{-1}) was taken in a conical flux and was heated with vigorous magnetic stirring. The hot solution of the salts was quickly transferred to the alkali medium and the final pH of the solution was maintained at about 10. The stirring was continued for about two hours at about 80 °C for complete digestion. To obtain a neutral pH condition, the co-precipitated particles were washed several times and finally filtered and dried

Table 1. Heat treatment schedules, lattice parameters including error, Curie temperatures, average particle sizes, blocking temperatures and magnetizations of $Ni_{0.2}Zn_{0.6}Cu_{0.2}Fe_2O_4$.

Annealing temperature	Lattice parameter		Average particle size (nm)		Curie temperature		Blocking temperature	Magnetization (A m^2 kg^{-1})	
(°C)	a (nm)	($\pm10^{-4}$ nm)	XRD[a]	TEM[c]	T_{Cp} (K)[d]	T_{Cf} (K)	T_B (K)[b]	90 K	RT
200	0.843 87	3.385	7	8	170	326	88	55.9	17.4
400	0.842 63	8.835	9	15	270	386	146	55.9	28.4
600	0.842 35	7.285	15	17	377	406	282	76.8	41.0
700	0.844 67	1.11	19	25	390	413	291	91.6	46.0
800	0.843 85	3.065	25	28	410	428	—	91.0	51.0
900	0.842 04	1.445	30	39	410	438	—	104.2	53.0

[a] Maximum error ±1 nm.
[b] Measured from maxima of χ'–T curves.
[c] Maximum error ±1 nm.
[d] Measured from Weiss plot.

at 100 °C for 12 h. The dried samples were annealed in air at various temperatures to obtain the desired mixed ferrite of different sizes. Table 1 shows the details of the annealing temperatures and corresponding particle sizes.

X-ray diffraction patterns of the ferrite samples were taken in an Xpert Pro Phillips x-ray diffraction unit with Cu Kα radiation ($\lambda = 0.154\,25$ nm) in the range of 2θ from 20° to 70°. TEM studies were carried out using a Hitachi H-600 transmission electron microscope (TEM) operating at 100 kV. Mössbauer effect measurements were carried out using a PC based spectrometer having a 1024 channel MCA card operating in the constant acceleration mode. All measurements were carried out in transmission geometry using a 10 mCi ^{57}Co source in an Rh matrix. The spectrometer was calibrated with a 12 μm thick high purity natural iron foil. Low temperature measurements were carried out by mounting the sample in the cold head of a closed cycle refrigerator (model CCS 850) supplied by M/s Janis Research Inc. with a special anti-vibration stand. No line broadening has been detected due to the expander vibration. The temperature of the sample was controlled with an accuracy of ±0.1 K using a temperature controller (Lake Shore). DC magnetization measurements at room temperature and at 90 K were carried out by a vibrating sample magnetometer (VSM) with maximum field 0.9 T (720 kA m^{-1}). AC hysteresis loops of the samples were observed by the inductive method at 37 Hz using the compensated coil technique, where acquisition is made by a 12 bit Nicolet digital oscilloscope, and integration was performed digitally. AC magnetic susceptibility measurements were carried out in a standard double coil arrangement. The measuring frequency and magnetic field were about 33 Hz and 8000 A m^{-1} respectively. The samples were taken in the form of pellets of about 8 mm diameter prepared by pressing the powder at a pressure of about 12 MPa. Measurements were made in the temperature range 80–450 K in a liquid nitrogen cryostat. The temperature was measured by a calibrated platinum resistance thermometer.

3. Results and discussion

3.1. XRD and TEM analysis

X-ray diffraction patterns of the samples with different sizes are shown in figure 1. The lattice parameters were obtained from the XRD pattern after performing Nelson–Riley–Taylor–

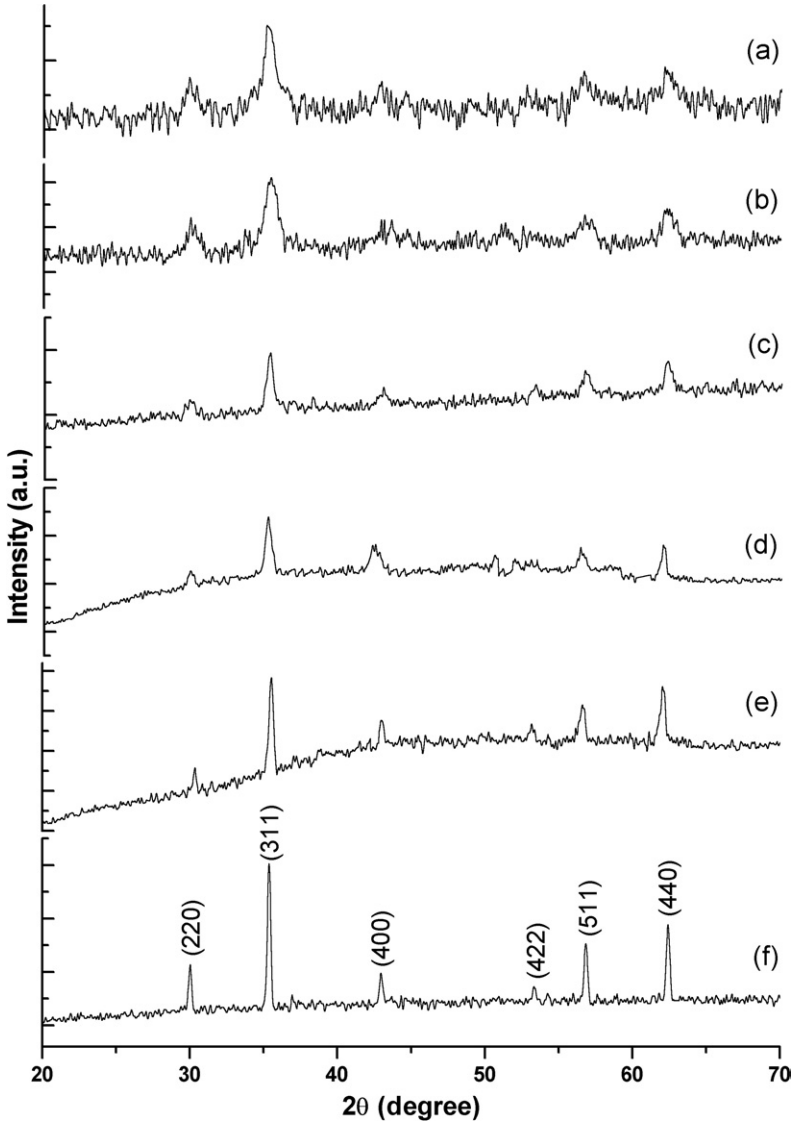

Figure 1. X-ray diffraction patterns of $Ni_{0.2}Zn_{0.6}Cu_{0.2}Fe_2O_4$ samples annealed at (a) 200 °C, (b) 400 °C, (c) 600 °C, (d) 700 °C, (e) 800 °C, and (f) 900 °C.

Sinclair correction in order to compensate peak shift due to sample offset. Lattice parameters together with their errors are listed in table 1. These lattice parameters confirm the formation of mixed spinel Ni–Zn–Cu ferrite phase. No peaks corresponding to any additional crystalline component were detected in the spinel nano-ferrites. It is interesting to note that the spinel ferrite phase has formed even at 200 °C without any peak corresponding to α-Fe_2O_3. The peaks of samples annealed at 200 and 400 °C are very broad because of the small size of crystallites, and due to these broad peaks the background emerges more intensely. However, by comparison to the pattern of figure 1(f) (corresponding to annealing at 900 °C), which shows all characteristic patterns of spinel, it is possible to distinguish (400) and (422) peaks in the noisy patterns.

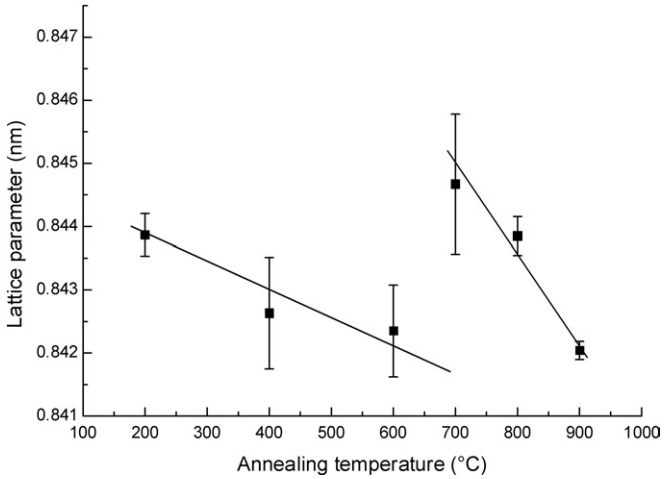

Figure 2. Variation of lattice parameters (including the error) with particle size.

The variation of lattice parameter with annealing temperature is displayed in figure 2. The lattice parameter slowly decreases with the increase of annealing temperature up to 600 °C, beyond which there is a sharp rise at about 700 °C, followed by a steep decrease in the range 700–900 °C. This sort of variation of lattice parameter with temperature may be attributed to redistribution of cations between tetrahedral and octahedral sites, with maximum cationic inversion occurring at about 700 °C.

The average particle sizes of all the heat-treated samples are evaluated from the line broadening of the (311) line using the Debye–Scherrer equation

$$\langle D\rangle_{(311)} = \frac{0.9\,\lambda}{\beta_{\frac{1}{2}}\cos\theta} \tag{1}$$

where $\langle D\rangle$ is the average particle size, λ is the wavelength of the incident x-ray and θ is the corresponding Bragg angle. Here $\beta_{\frac{1}{2}} = \sqrt{(\beta_{\frac{1}{2}})_0^2 - b_0^2}$, where $(\beta_{\frac{1}{2}})_0$ is the full width at half maximum (FWHM) of the (311) peak and b_0 is the same for large crystallites. The value of $(\beta_{\frac{1}{2}})_0$ was obtained from the fitting of the (311) peak to the Lorentzian function. The uncertainties in the particle size determination were estimated from the errors in the fitting procedures, which lie in the range ± 1 nm. The average particle sizes of all the heat-treated samples are in the range 7–30 nm (table 1).

Figure 3 displays a few representative transmission electron micrographs of the ferrite nanoparticles and the corresponding histograms are displayed in figure 4. It has been observed that particles prepared with annealing temperatures up to 600 °C are somewhat agglomerated in nature (figures 3(a)–(c)). The degree of agglomeration decreases with the increase of annealing temperature and particles prepared by heating the as-prepared samples at 700 °C (figure 3(d)) are discrete and mostly spherical. The average particle sizes estimated from the TEM studies are presented in table 1. These values are in good agreement with those values obtained from XRD analysis using the Debye–Scherrer equation. In the remainder of the text the particle sizes mentioned are the values estimated from XRD analysis.

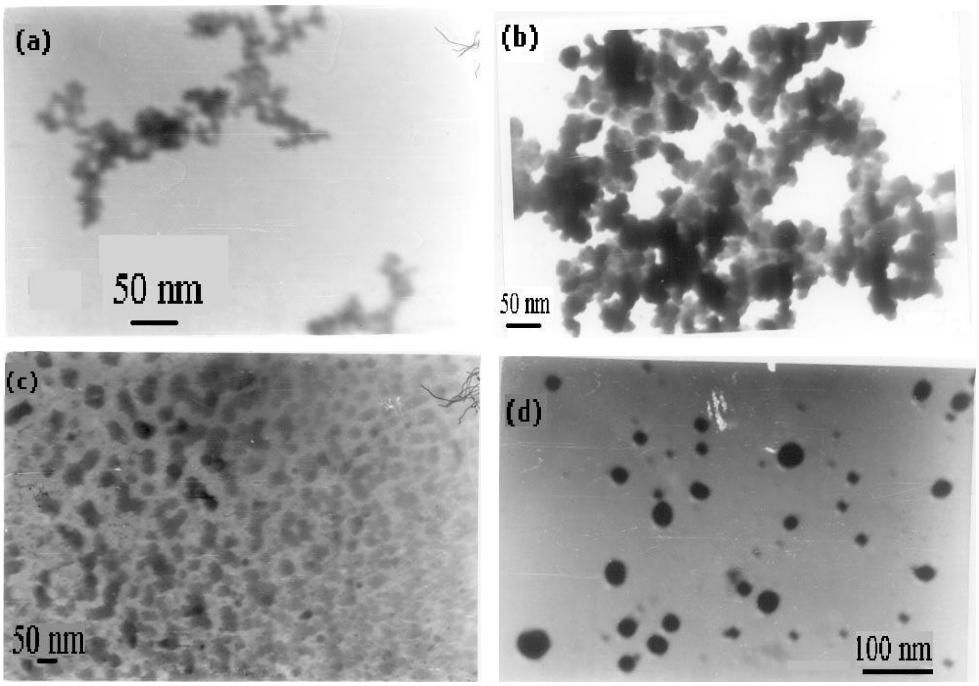

Figure 3. Transmission electron micrographs of $Ni_{0.2}Zn_{0.6}Cu_{0.2}Fe_2O_4$ annealed at (a) 200 °C, (b) 400 °C, (c) 600 °C, and (d) 700 °C.

3.2. Mössbauer analysis

Mössbauer spectra recorded at room temperature of the samples having different particle sizes are displayed in figure 5. The experimental data were fitted with least squares fitting programs LGFIT2 [16] and NORMOS [17] for discrete sites and for distributions respectively. In all the discrete fittings, Lorentzian line shapes were assumed. Mössbauer spectra of the samples having particle sizes 7 and 9 nm respectively show prominent doublets (figures 5(a) and (b)) with some broadening near the shoulders. These spectra were fitted with a distribution of quadrupole doublets. The doublets were assigned to ultrafine ferrite particles undergoing SPM relaxation, whereas the broadening near the shoulders is due to larger particles in the samples showing incomplete collapse of the sextet pattern. The probability distributions of the quadrupole splitting obtained from the fit are shown in figures 5(a′) and (b′). The values of isomer shift (IS) and quadrupole splitting (QS) extracted from the fit are shown in table 2. The IS values confirm the Fe^{3+} valence state of iron in the ferrites whereas the QS values are indicative of substantial electric field gradient (EFG) around the ^{57}Fe probe nuclei. Both the samples with average size 15 and 19 nm showed a doublet with broadened shoulder along with a collapsing sextet (figures 5(c) and (d)). These spectra were fitted with a distribution of hyperfine fields along with a discrete quadrupole doublet. The probability distribution of the hyperfine magnetic field $P(H)$ as a function of the internal hyperfine magnetic field H are shown in figures 5(c′) and (d′). The broad humps observed in the region 15.0–40.0 T without any well defined peak indicate incomplete magnetic ordering due to the broad size distribution present in these samples. The hyperfine parameters extracted from the fit are tabulated in table 2. Mössbauer spectra of the samples having particle sizes of 25 and 30 nm (figures 5(e) and (f)) showed typical sextet patterns with the signature of magnetic relaxation. These spectra

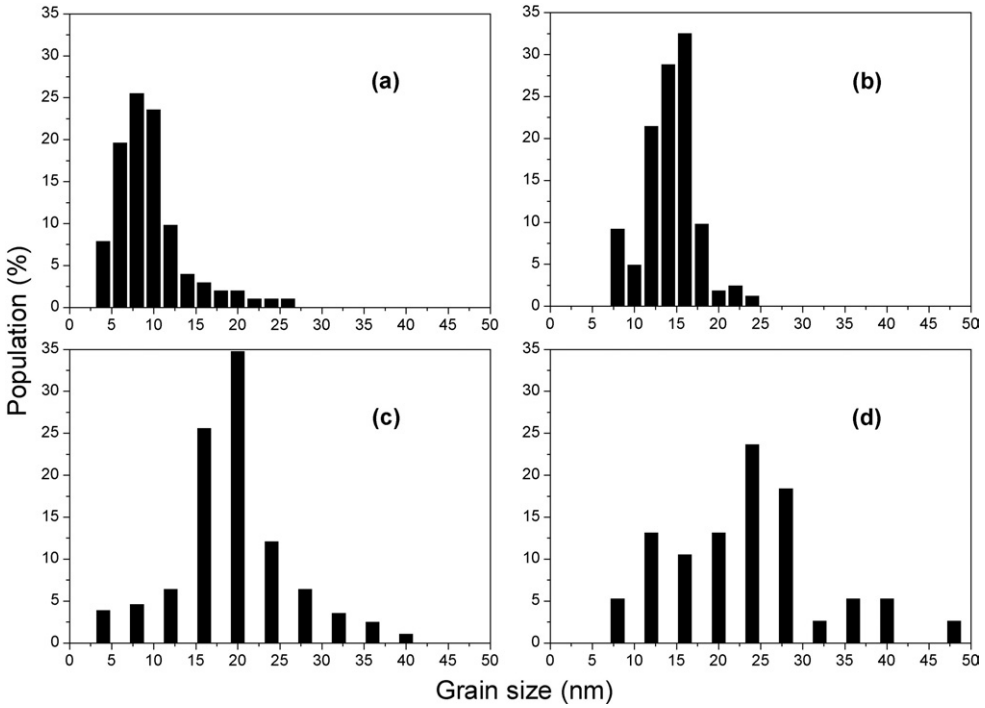

Figure 4. Histograms of $Ni_{0.2}Zn_{0.6}Cu_{0.2}Fe_2O_4$ annealed at (a) 200 °C, (b) 400 °C, (c) 600 °C, and (d) 700 °C.

were fitted with distribution of hyperfine fields, and the probability distributions ($P(H)$ versus H) are shown in figures 5(e′) and (f′). It may be mentioned here that, though distribution of hyperfine parameters usually gives a qualitative fit, in the present case this method was adopted as it gave a much better fit to the experimental points than the fit by assuming discrete sites. Attempts to fit one discrete doublet each for the samples with size 7 and 9 nm, and one doublet and a relaxing sextet for the samples with sizes 15, 19, 25 and 30 nm, gave very large χ^2 values and was unacceptable. This essentially was due to very broad asymmetric lines observed in the present samples, which could be due to distribution of particle sizes resulting in continuous variation of the electric field gradient and hyperfine field at the ^{57}Fe nuclei.

To confirm the presence of SPM particles, Mössbauer spectra of the samples were recorded down to 20 K. Figure 6 shows a typical spectrum of the sample with average size 9 nm recorded at different temperatures. It is clear from the figure that as the temperature is lowered a sextet pattern emerges at the expense of the doublet. This confirms that the doublets observed at room temperature were due to finer particles of ferrites undergoing SPM relaxation. At 20 K, a broad sextet is observed and the spectrum was fitted with two discrete sextets. The hyperfine parameters obtained from the fit are shown in table 3. The sextet with lower IS (0.50 mm s^{-1}) and QS (0.04 mm s^{-1}) is attributed to Fe^{3+} ions in tetrahedral (A) sites. The other one with higher IS (0.52 mm s^{-1}) and QS (0.03 mm s^{-1}) is attributed to Fe^{3+} ions in octahedral (B) sites.

3.3. Magnetic properties

The measured values of Curie temperatures of all the samples with different particle sizes are shown in table 1. The highest value of T_c (438 K) was obtained for the sample with particle

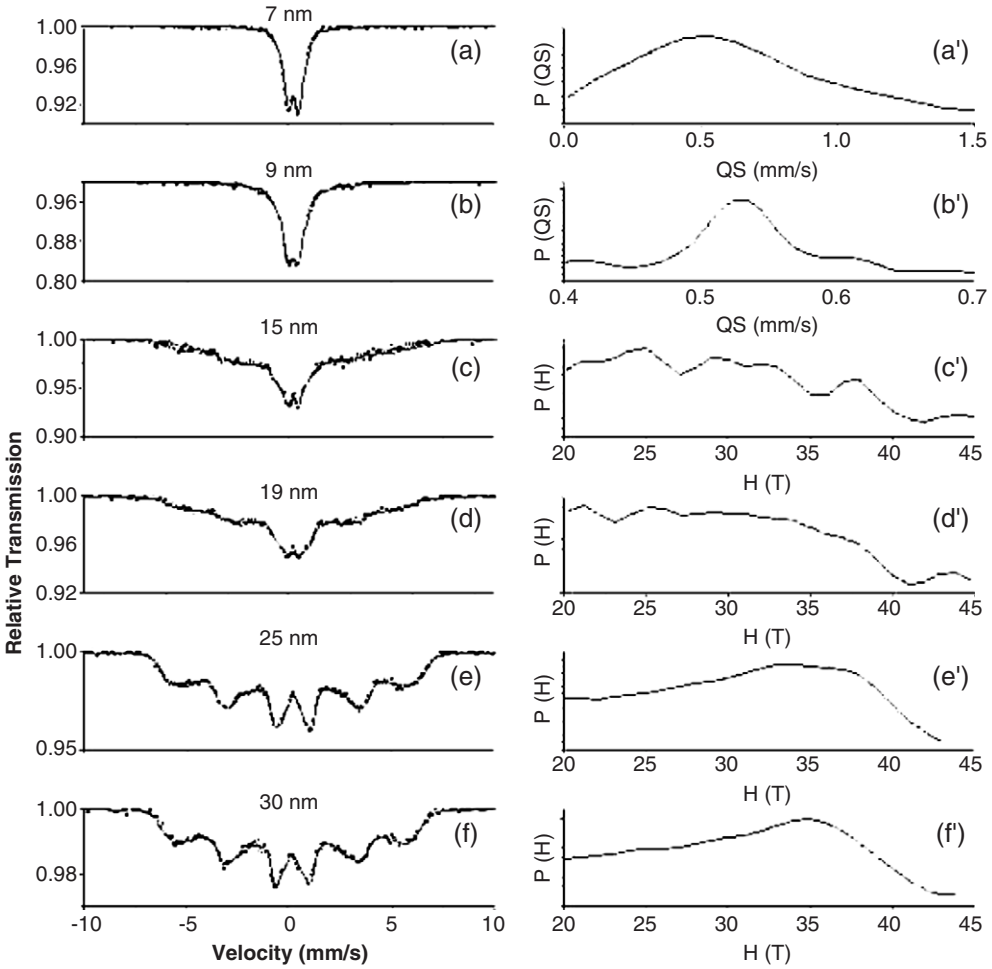

Figure 5. Room temperature Mössbauer spectra and probability distributions of $Ni_{0.2}Zn_{0.6}Cu_{0.2}Fe_2O_4$ having different particle sizes.

size 30 nm, which is comparable to the corresponding value of Ni–Zn ferrite (425 K) [18, 19]. Figure 7 displays the variation of DC magnetization of all the samples having different particle sizes with applied magnetic field. The DC magnetization curves of samples up to particle size 19 nm show typical characteristic behaviour of SPM particles where magnetizations slowly approach saturation. In these cases the maximum applied field of 720 kA m^{-1} is still not enough to obtain the saturation magnetization value at room temperature. But for the samples with sizes 25 and 30 nm, which are obtained after annealing the as-prepared sample at 800 and 900 °C respectively, saturation magnetization was clearly obtained above 150 kA m^{-1}. This sort of behaviour is not the characteristic behaviour of SPM particles. Though room temperature Mössbauer spectra of these samples (figures 5(e), (f)) indicate the presence SPM particles together with the ferrimagnetically ordered particles, the corresponding VSM curves suggest that the magnetic behaviour is mostly controlled by the ferrimagnetic fraction as the former has no signature in the DC magnetization curve. The saturation magnetization values (σ_s @ 720 kA m^{-1}) measured at room temperature (RT) and 90 K are mentioned in table 1.

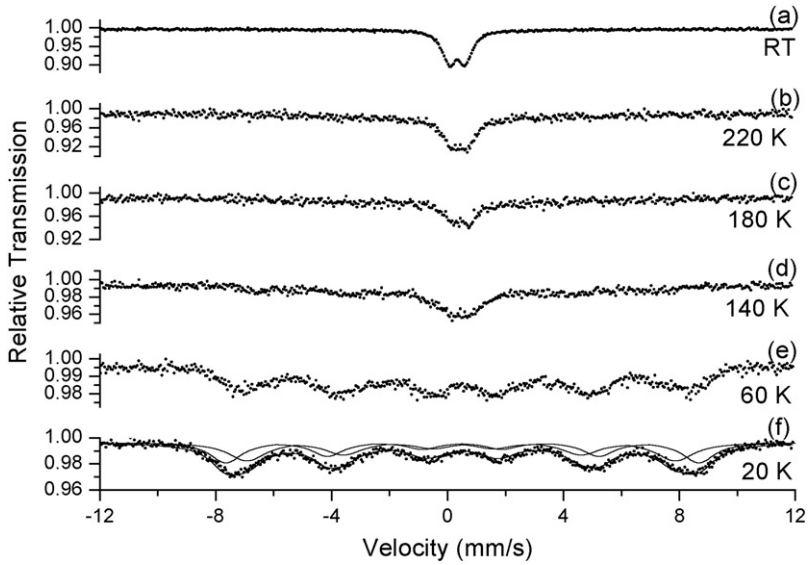

Figure 6. Mössbauer spectra of $Ni_{0.2}Zn_{0.6}Cu_{0.2}Fe_2O_4$ with particle size 9 nm at (a) room temperature (RT), (b) 220 K, (c) 180 K, (d) 140 K, (e) 60 K, and (f) 20 K.

Table 2. Hyperfine parameters of $Ni_{0.2}Zn_{0.6}Cu_{0.2}Fe_2O_4$ extracted from the fitting of Mössbauer spectra recorded at room temperature. (Note: IS = isomer shift (relative to natural iron), QS = quadrupole splitting (2ε), H_{int} = internal magnetic field, D = doublet, S = sextet.)

Particle size (nm)	Spectra fitted with	IS[a] (mm s^{-1}) (±0.02)	QS[a] (mm s^{-1}) (±0.02)	H_{int}[a] (T) (±0.2)
7	D	0.22	0.77	—
9	D	0.25	0.53	—
	D	0.26	0.40	—
15	S	0.13	0.36	21.2
	D	0.26	0.52	—
19	S	0.15	0.16	21.2
25	S	0.21	0.01	25.0
30	S	0.12	0.04	25.0

[a] In the case of fitting the distribution function the values tabulated are the average values.

Table 3. Hyperfine parameters extracted from the fitting of the Mössbauer spectrum recorded at 20 K of $Ni_{0.2}Zn_{0.6}Cu_{0.2}Fe_2O_4$ with average particle size 9 nm. (Note: IS = isomer shift (relative to natural iron), QS = quadrupole splitting, RA = relative area.)

Site	IS (mm s^{-1}) (±0.02)	QS (mm s^{-1}) (±0.02)	H_{int} (T) (±0.2)	RA (%) (±3%)
A	0.50	0.04	45.9	52
B	0.52	0.03	50.7	48

Figure 8 displays the variation of specific saturation magnetization value (σ_s @720 kA m^{-1}) as a function of particle sizes of the sample measured at room temperature (RT) and at 90 K.

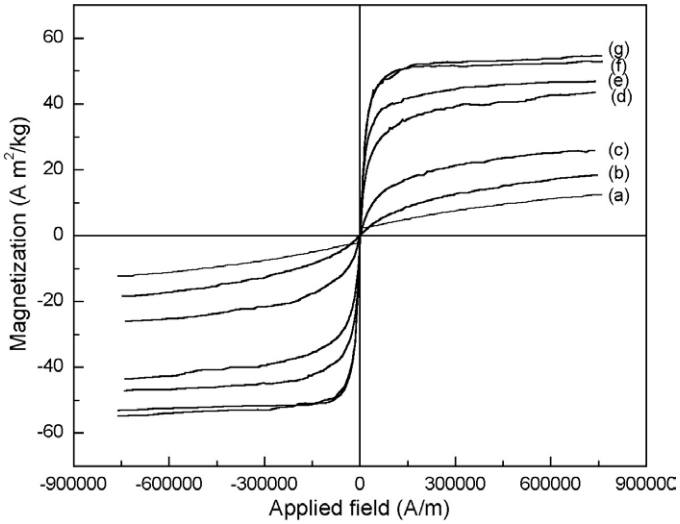

Figure 7. Variation of magnetization with magnetic field of $Ni_{0.2}Zn_{0.6}Cu_{0.2}Fe_2O_4$ samples with different particle sizes: (a) as prepared, (b) 7 nm, (c) 9 nm, (d) 15 nm, (e) 19 nm, (f) 25 nm, and (g) 30 nm.

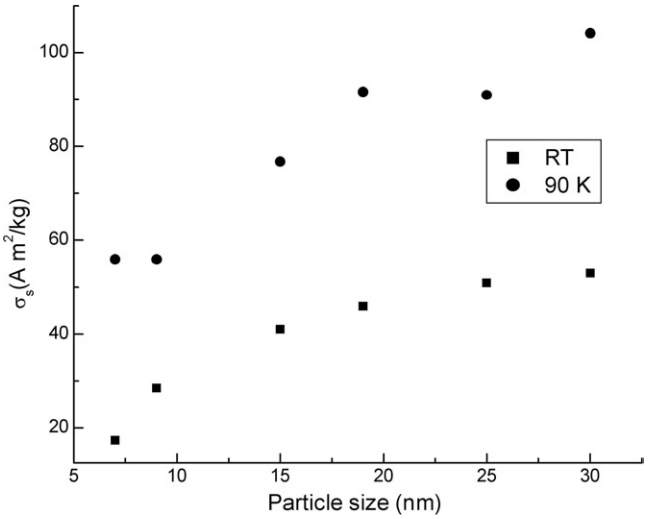

Figure 8. Specific saturation magnetization as a function of particle size.

The values of specific saturation magnetizations measured at RT are not reliable since the SPM samples are not fully saturated. In contrast, at 90 K, all samples are in the blocked regime and fully saturated under a field of 720 kA m^{-1}. It is clear from these data that annealing up to 400 °C (particle size 9 nm) does not affect sensitively the value of the magnetization, σ_s (90 K) $\approx$ 56 A m^2 kg^{-1}. Annealing above 600 °C (particle size 15 nm) results in a sharp increase of saturation magnetization value to above 90 A m^2 kg^{-1}. This effect is consistent with the sharp change in the variation of lattice parameter with temperature (figure 2) observed in the same temperature range, which indicates cationic inversion at this temperature. As Zn^{2+} is the biggest ion in this system, it is probable that it goes to the octahedral (B) site during synthesis

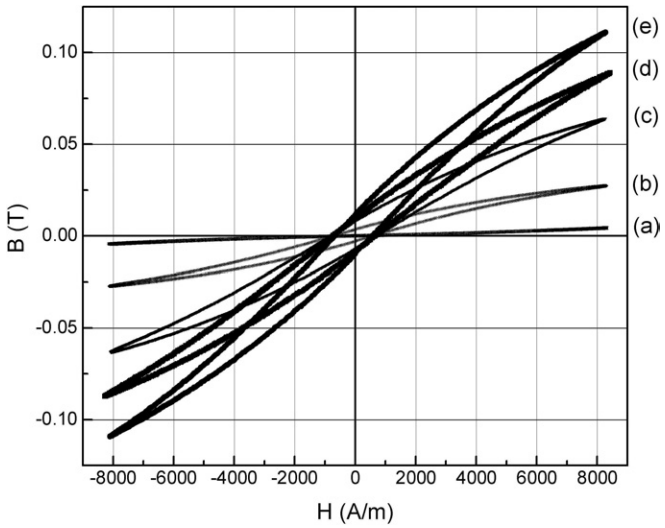

Figure 9. AC hysteresis loops of $Ni_{0.2}Zn_{0.6}Cu_{0.2}Fe_2O_4$ samples with different particle sizes: (a) 9 nm, (b) 15 nm, (c) 19 nm, (d) 25 nm, (e) 30 nm.

according to the inverse spinel structure. In the spinel system, Fe^{3+} in B (octahedral) and A (tetrahedral) sites interacts antiferromagnetically and spins are compensated, resulting in no net magnetization. Upon annealing, the spinel becomes a mixed one and Zn^{2+} goes to the A site replacing Fe^{3+}, which eventually goes to the octahedral B site, which is more favourable from the electronic point of view. The excess Fe^{3+} ions in the B site interact partly ferromagnetically with other Fe^{3+} ions, resulting in an increase of magnetization by up to 85%.

The hysteresis loops observed at 37 Hz of all the samples with different particle sizes are shown in figure 9. The coercive field for the samples with particle size 9 nm is interestingly very low, only 156 A m^{-1}. This low value suggests that most of the particles present in the sample are superparamagnetic, which is also in good agreement with the findings of room temperature Mössbauer measurement (figure 5(b)). The variation of coercive field (H_c) with the particle size is shown in figure 10. The value of H_c increases with the increases of particle size up to 19 nm, beyond which it decreases. In the present samples the values of H_c are low compared to nano-crystalline $Ni_{0.35}Zn_{0.65}Fe_2O_4$ as observed by Caizer and Stefanescu [20]. For example, for the sample $Ni_{0.35}Zn_{0.65}Fe_2O_4$ with particle size 14.6 nm the value of H_c was more than 800 A m^{-1}, whereas in our present sample with particle size 15 nm the value of H_c is ∼650 A m^{-1}. This difference is attributed to the difference in the composition since a small fraction of Cu in Ni–Zn ferrite is known to lower the anisotropy constant. In the present work, the grain size of all the samples is smaller than the corresponding single domain critical size $D_{SD} \approx 4\sqrt{3}\ell_{ex} = 70$ nm (with $\ell_{ex} = \sqrt{2\mu_0 A/J_S^2}$, the exchange constant $A \approx 5$ pJ m^{-3} and $J_S = 0.35$ T for the present composition). Hence the increase in grain size results in an increase of relaxation time and eventually the coercivity. The substantially lower coercivity of the sample annealed at 900 °C compared to that annealed at 800 °C (both being in ferrimagnetic state) could be due to a better crystallinity.

The thermal variations of the real part of AC magnetic susceptibilities (χ') of the samples with different particle sizes are displayed in figure 11. From the observed variations it is clear that in all the cases except for the samples with particle sizes 25 and 30 nm χ' passes through a maximum, a typical phenomenon found in nanoparticles undergoing SPM relaxation. The

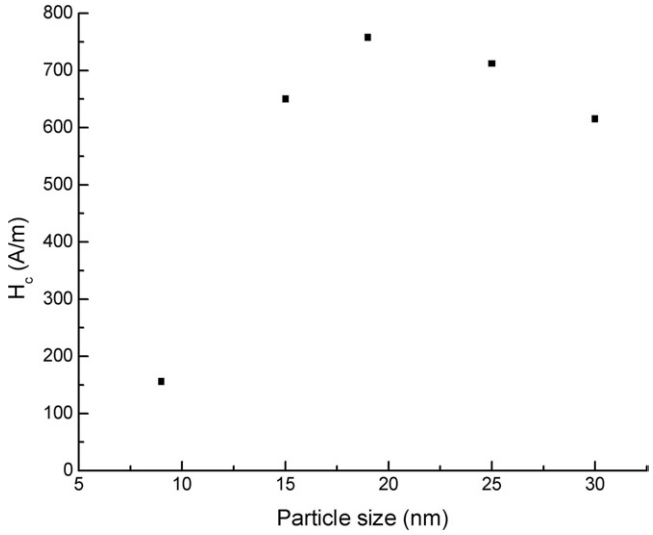

Figure 10. Variation of coercive field (H_c) with the increase of particle size.

temperatures where maxima are observed are the so-called blocking temperatures (T_B) for the particles with different sizes. Here the blocking temperature is defined as the temperature at which the magnetic relaxation time of the nanoparticles equals the experimental timescale of the AC magnetic susceptibility measurements (τ_s) and is given by

$$T_B = \frac{K_A V}{k_B \ln\left(\frac{\tau_s}{\tau_0}\right)} \tag{2}$$

where K_A is the anisotropy constant, V is the volume of the magnetic nanoparticle, k_B is the Boltzmann constant and τ_0 is the inverse of the natural frequency of the gyromagnetic precession. The blocking temperatures estimated from the maxima of χ' versus T curves of all samples, except those with sizes 25 and 30 nm, are presented in table 1.

A close inspection of the χ'–T graph reveals that the nature of variations of χ'–T curves for the samples with particle sizes 25 and 30 nm are not the typical characteristic of SPM particles. In these cases χ' decreases very sharply above 352 and 372 K respectively. This type of transition may be attributed to ferrimagnetic to paramagnetic transition. For these samples, room temperature Mössbauer spectra have some relaxation effects due to SPM particles but their strength is considerably weak compared to that of ordered particles. Thus for these two samples the magnetic properties are mainly governed by the ordered particles. This is also supported by our VSM curves (figure 7), which have the typical Langevin shape up to 19 nm only. The coercive field values obtained from digital hysteresis loops suggest that all samples contain a fraction of particles, which are not relaxed within the measuring time. This can be attributed to size distribution or, more probably for samples with smaller average grain size, to clustering of particles coupled by dipolar interaction. The continuous increase in coercive field with grain size is consistent with strengthening of blocking.

To have further insight concerning the origin of the coercive field of the superparamagnetic sample, $1/\chi'$ values above the blocking temperature have been fitted using the Curie–Weiss law, $1/\chi' = (T - T_{Cp})/C$, where C is the Curie constant and T_{Cp} is the paramagnetic Curie temperature, which, in a ferrimagnetic sample, is only a few kelvin below the ferrimagnetic Curie point T_{Cf} obtained from the drop to zero of χ'. For superparamagnetic samples, it is

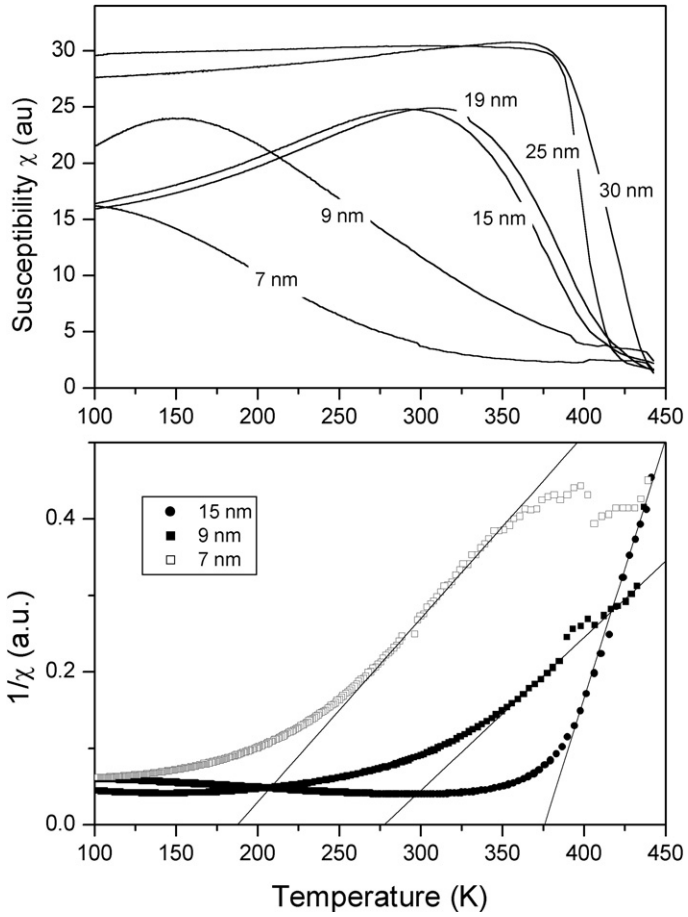

Figure 11. AC magnetic susceptibilities (χ') of $Ni_{0.2}Zn_{0.6}Cu_{0.2}Fe_2O_4$ annealed at different temperatures and inverse of χ' versus T including fitting curves.

theoretically equal to zero. However, nonzero T_{Cp} values are found for the samples up to size 19 nm. This is attributed to the dipole–dipole interactions resulting in a non-zero mean field. The 7 nm sample exhibits a paramagnetic Curie temperature of 170 K, whereas the ferrimagnetic one is about 326 K (see table 1) and the blocking temperature is 88 K. With increasing grain size, T_{Cp} becomes closer to T_{Cf} and finally it is only a few tens of kelvin below the latter. It is to be noted that T_{Cp} is not connected to T_B since they depend on the strength of dipolar interactions ($T_{Cp} \propto DJ_0^2$, where J_0 is the spontaneous magnetization at 0 K) and anisotropy ($T_B \propto D^3K_A$) respectively. Using the blocking temperatures obtained from AC magnetic susceptibility measurements and average particle sizes estimated from XRD spectra, the anisotropy energy constants of all the samples up to particle size 19 nm were evaluated from equation (2). Here τ_s is the timescale of the AC susceptibility measurements, which was ~30 ms, and the value of τ_0 has been taken as 10^{-10} s [1, 21, 22]. With these numerical values, equation (2) becomes $K_AV = 19.62k_BT_B$, which may be considered as the condition for superparamagnetism in the present case. Above the blocking temperature (T_B) particles satisfying this relation will relax during the timescale of the AC measurements, and below the blocking temperature the particles will be in a blocked state and the anisotropy energy

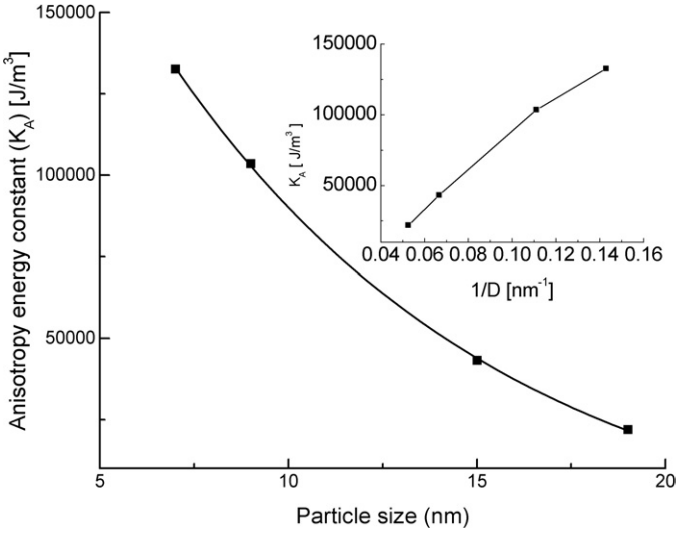

Figure 12. Variation of anisotropy energy constant (K_A) with the variation of particle size.

constant can be evaluated from the relation $K_A = (19.62k_BT_B)/V$. The variation of anisotropy energy constant with the average particle size is displayed in figure 12. The value of anisotropy energy constant decreases sharply with the increase of particle size. In the case of particles with lower sizes, the values of anisotropy energy constants are much higher compared to the bulk values [22] and this is usually explained by the surface anisotropy contribution. As the particle size decreases more atoms or ions appear on the surface of the nanoparticles, exhibiting higher contribution to the surface anisotropy [22, 24, 25]. Again, if we plot the values of K_A as a function of $1/D$, where D is the average particle size, then it gives a linear variation (shown in the inset of figure 12). This is usually attributed to surface anisotropy. However, it is to be noted that the evaluated anisotropy energy constants are the values at their respective blocking temperatures. For example, the evaluated anisotropy energy constant of samples with particle size 7 nm is 133 kJ m^{-3} at $T_B = 88$ K ($\approx 0.25T_C$) and this value decreases to 21.9 kJ m^{-3} at 291 K ($\approx 0.75T_C$) for the sample with particle size 19 nm. The anisotropy energy constant is highly sensitive to temperature as in the case of the bulk, the value at room temperature (300 K) may increase several-fold (more than fivefold) at low temperature (100 K) [23]. Also, anisotropy must be strongly affected by change in ionic distribution. Thus, in the present case, the decrease of anisotropy energy constant is not directly correlated to particle size but rather to thermal variation (as they are obtained at different temperatures) and order. The high values of anisotropy energy constants in ferrite nanoparticles were also reported by others [22, 26].

4. Conclusions

Nanoparticles of $Ni_{0.2}Zn_{0.6}Cu_{0.2}Fe_2O_4$ have been prepared by the standard co-precipitation method. Annealing of the as prepared dried precipitate in air at various temperatures from 200 to 900 °C results in the formation of mixed spinel ferrite phase with sizes lying in the range 7–30 nm. The calculated values of particle sizes using the Debye–Scherrer equation from the (311) peak of the XRD spectra are in good agreement with those values directly obtained from TEM observations. The calculated values of lattice parameters of the samples with different particle sizes suggest the redistribution of cations in different sites (tetrahedral

and octahedral) with the increase of particle sizes and the maximum cationic inversion occurs at annealing temperature 700 °C. The particles with sizes up to 15 nm are agglomerated in nature and above this the particles are dispersed. AC magnetic susceptibility and Mössbauer measurements clearly show the presence of superparamagnetic relaxation in all the samples. Blocking temperature measured from AC magnetic susceptibility data and the magnetization curves of the samples both show that particles are SPM at room temperature up to 19 nm. The values of specific saturation magnetization increase with annealing temperature as a result of non-equilibrium ionic distribution in nanoparticles synthesized by co-precipitation. The hysteresis loops of the samples with different particle sizes give the coercive fields, which increase up to a critical size of 19 nm, beyond which they decrease. The values of H_c are also interestingly low compared to the same reported for the Ni–Zn-ferrite nanocrystalline system [21].

Acknowledgments

One of the authors (P K Chakrabarti) wishes to thank the University Grants Commission (India) for financial assistance for this work.

References

[1] Dormann J L and Fiorani D (ed) 1992 *Magnetic Properties of Fine Particles* (Amsterdam: North-Holland)
[2] Wang C, Zhang X M, Qian X F, Xie J, Wang W Z and Qian Y T 1998 *Mater. Res. Bull.* **33** 1747
[3] Bentivegna F, Nyvlt M, Ferre J, Jamet J P, Brun A, Visnovsky S and Urban R 1999 *J. Appl. Phys.* **85** 2270
[4] Berkowitz A E, Kodama R H, Makhlouf S A, Parker F T, Spada F E, McNiff E J Jr and Foner S 1999 *J. Magn. Magn. Mater.* **196/197** 591
[5] Nakamura T 2000 *J. Appl. Phys.* **88** 348
[6] Kim W C, Kim S J, Lee S W and Kim C S 2001 *J. Magn. Magn. Mater.* **226–230** 1418
[7] Yue Z X, Zhou J, Wang X H, Gui Z L and Lee L T 2001 *J. Mater. Sci. Lett.* **20** 1327
[8] Brabers V A M 1995 *Handbook of Magnetic Materials* vol 8, ed K H J Buschow (Amsterdam: North-Holland) p 189
[9] Zhang Z J, Wang Z L, Chakoumakos B C and Yin J S 1998 *J. Am. Chem. Soc.* **120** 1800
[10] Chen Q, Rondinone A J, Chakoumakos B C and Zhang Z J 1999 *J. Magn. Magn. Mater.* **194** 1
[11] Nath B K, Chakrabarti P K, Das S, Kumar U, Mukhopadhyay P K and Das D 2004 *Eur. Phys. J.* B **39** 417
[12] Nomura T and Takaya M 1987 *Hybrids* **3** 15
[13] Yue Z, Li L, Zhou J, Zhang H, Ma Z and Gui Z 2000 *Mater. Lett.* **44** 279
[14] Sung H M, Chem C J, Ko W S and Lin H C 1994 *IEEE Trans. Magn.* **30** 4906
[15] Su H, Zhang H, Tang X and Xiang X 2004 *J. Magn. Magn. Mater.* **283** 157
[16] von Meerwall E 1975 *Comput. Phys. Commun.* **9** 117
[17] Brand R A 1987 *Nucl. Instrum. Methods* B **28** 398
[18] Verma A, Goel T C, Mendiratta R G and Kishan P 2000 *J. Magn. Mater.* **208** 13
[19] Globus A, Pascard H and Cahan V 1977 *J. Physique Coll.* **38** C1 163
[20] Caizer C and Stefanescu M 2002 *J. Phys. D: Appl. Phys.* **35** 3035
[21] Vincent E, Hammann J, Prené P and Tronc E 1994 *J. Physique* I **4** 273
[22] Moumen N and Pileni M P 1996 *J. Phys. Chem.* **100** 1867
[23] Soshin C 1964 *Physics of Magnetism* (Malabar, FL: Krieger) p 140
[24] Kodama R H, Berkowitz A E, McNiff E J and Foner S 1996 *Phys. Rev. Lett.* **77** 394
[25] Muroi M, Street R, McCormick P G and Amighian J 2001 *Phys. Rev.* B **63** 184414
[26] Tung L D, Kolesnichenko V, Caruntu G, Caruntu D, Remond Y, Golub V O, O'Connor C J and Spinu L 2002 *Physica* B **319** 116